Comparative study of land-use classification through multispectral instruments by using accuracy assessment and area estimation techniques over Mardan district, Pakistan

Muhammad Junaid[1,2,3], Sun Jianguo[1,2,3*], Mirza Waleed[4], Azhar Khan[5]

[1] Faculty of Geomatics, Lanzhou Jiaotong University, Lanzhou 730070, Gansu, China；
[2] National-Local Joint Engineering Research Center of Technologies and Applications for National Geographic State Monitoring, Lanzhou 730070, Gansu, China；
[3] Gansu Provincial Engineering Laboratory for National Geographic State Monitoring, Lanzhou 730070, Gansu, China;
[4] Department of Geography, Hong Kong Baptist University, Hong Kong SAR;
[5] Department of Geology, The University of Haripur, Pakistan
*Corresponding author: Sun Jianguo(sunjguo@mail.lzjtu.cn)

Abstract

Land use and land cover (LULC) mapping is important for various activities ranging from proper resource allocation to policy planning. Freely available satellite data from multispectral instruments has opened wide doors for their applications in urban planning, natural resource monitoring, and change analysis. Previously, many researchers have individually used multispectral instruments, i.e., Sentinel-2 (10m), Gaofen-6 (16m), and Landsat-8 (30m) for land-use classification, but till now, no study has evaluated the efficiency of these three instruments in land-use classification. So this study evaluated the comparison of these instruments using accuracy assessment and area esitimation by machine learning classification over the Mardan district of Pakistan. The study revealed that Sentinel-2 secured the highest accuracy but at the same time showed confusion between buildup and barren classes. Landsat-8, with the least accuracy, performed exceptionally well for mapping agricultural areas, rangeland, and forest land. Lastly, Gaofen-6 was considered far better in terms of reliable outcomes for mapping city urban areas, where it showed good outcomes. In terms of accuracy assessment, Sentinel-2 stood first with Overall Accuracy (OA) of 0.89 and Kappa (K) of 0.85, then Gaofen-6 with OA equals to 0.80 and K equals to 0.79, while Landsat-8 stood last with OA equals to 0.76 and K equals to 0.70. The results of area estimation revealed that Gaofen-6 (12856 ha) estimated the most accurate area for the buildup class, followed by Landsat-8 (11169 ha), and Sentinel-2 (8307 ha). It was observed that in Sentinel-2 based classification, urban areas were misclassified as barren in nearby city parts. In the end, the study concludes that the efficiency of land-use primarily depends on the purpose of research. For forestland, agriculture, rangeland, and barren land LULC classes, both Sentinel-2 and Gaofen-6 showed promising results, whereas for water class only, Geofen-6's results seem quite accurate. This study revealed that Gaofen-6 showed promising results compared to Sentinel-2 and Landsat-8.

Keywords: LULC; Machine Learning; sentinel-2; landsat-8; Gaofen-6

I. Introduction

Land use/land cover (LULC) is a fundamental and classical concept required to understand the interaction between humans and the physical environment.The land cover defines the physical and biological characteristics of the Earth's surface, including agricultural land, water bodies, vegetative cover, bare land, and built-up areas. In contrast, land use refers to how humans utilise and manage the natural environment or land (ED Chaves et al., 2020). Over recent decades, the pattern of land use and land cover has undergone unprecedented changes. The pace of land use and land cover (LULC) change has multiplied as a result of economic and industrial development, as well as rapid and uncontrolled population expansion, particularly in developing nations, during the end of the twentieth century and the beginning of the twenty-first (Talukdar et al., 2020).

The various effects of change in LULC over large areas include loss of vegetation cover, loss of biodiversity, climate change, carbon emissions, environmental pollution, and changes in hydropower systems (Mridha et al., n.d.). The Climate Research Committee of the National Council stated that the pattern of LULCs

---

has a significant impact on Earth's radiation balancing because LULC variations affect evaporation, transpiration, and heat flow on the ground surface. That is why understanding LULC trends and monitoring the changing environment on a global to local scale is critical for scientists and practitioners (Cai et al., 2019). Since quantitative assessment of LULC change is one of the most effective means of understanding and managing land conversion (Talukdar et al., 2020), LULC data can help us understand how intertwined human–environmental systems are (ED Chaves et al., 2020). Therefore, researchers need to maintain an up-to-date, objective, and highly accurate and reliable LULC map (Gudmann et al., 2020).

The value of precise LULC data has grown in recent years to support the implementation of policies connected to natural resource management and environmental issues such as food security, climate change, deforestation, and agricultural dynamics. It emphasises the importance of accurate mapping for long-term development (ED Chaves et al., 2020). Mapping and evaluating land cover and land use are essential for many environmental and mapping applications. Land cover mapping and monitoring have long been seen as a significant scientific goal. The data generated can be used to assist ecological and atmospheric models, decision-making procedures, and so on (Topalolu et al., 2016a). LULC information and its spatial distribution patterns are vital for a wide range of research topics, especially in urban studies with diverse classes, as well as maintenance and development programs.LULC change has been viewed as a fundamental cause of global environmental change by influencing the land surface. Urban borders, river basins, wetlands, and agricultural areas are frequently exposed to LULC changes, mainly by reducing forest cover to allow for agricultural extension, urbanization, and industrialization, among other things. Land cover is rapidly changing in metropolitan areas, with the conversion from agricultural/fallow to concrete forest resulting in urban sprawl. Understanding numerous environmental issues associated with urban and adjacent environments requires an examination of LULC and its change (Pandey et al., 2021). Therefore, precise and up-to-date LULC information is valuable for a sustainable ecosystem (Sekertekin et al., 2017).

In recent decades, remote sensing has become one of the most widely used sources for LULC analysis. In mapping LULC and analysing their dynamics, remote sensing has been extensively employed, frequently combined with a Geographic Information System (GIS) (Pandey et al., 2021a). Mapping is done utilising accessible records, field surveys, and maps in traditional methods. It is a direct method of mapping in which the map can be created at various scales and with varying degrees of detail. As a result, traditional methods are a manpower-intensive, time-consuming, and costly approach to mapping large areas. Furthermore, the resulting maps quickly become obsolete in rapidly changing ecosystems, and there is a risk of subjectivity in the mapping (Vivekananda et al., 2021). On the other hand, remotely sensed data-based mapping of LULC is relatively inexpensive, geographically broad, multi-temporal, efficient, and time-saving (Talukdar et al., 2020). Satellite images and remote sensing have several advantages, including an overall perspective and the ability to describe phenomena utilising diverse sections of the electromagnetic spectrum (Ghayour et al., 2021). Remote sensing is a powerful technique for extracting accurate spatial data and LULC distribution over time (Pandey et al., 2021a). Previously, the spatial resolution of satellite data was lower than that of maps produced by terrestrial surveys. Satellites now deliver data at multiple spatial and temporal scales because of advancements in remote sensing (R.S.) techniques and microwave sensors. Compared to other methods such as field surveys, R.S. allows for the speedy capture of information on LULC at a significantly lower cost. For LULC mapping, remote sensing data offers the advantages of multi-temporal availability and high spatial coverage (Talukdar et al., 2020).

The interest in land use and land cover (LULC) maps has risen dramatically in recent years, owing in part to the increasing availability and accessibility of free satellite imagery. Satellite data with medium to high resolutions became more available as remote sensing technology advanced (Fu et al., 2020). The use of remotely sensed datasets is determined by the user's needs, purpose, and type of landscape evaluation. Other considerations such as geographical coverage, spatial and spectral resolution, temporal coverage, and Synthetic Aperture Radar (SAR) data all play a role in deciding which data to use for a given sort of study (Pandey et al., 2021a). Multispectral and multi-temporal high-and medium-spatial-resolution satellite images have appeared recently as key tools for assessing vegetation cover, forest degradation, and urban growth expansion (Güler et al., 2007). For analysing LULC changes in large cities, high-resolution satellite images or aerial imagery are essential. However, such datasets are inadequate (Gadrani et al., 2018). However, for LULC classification, medium-resolution data (10–30 m) such as Landsat, Sentinel, and Gaofen-8 have been utilised worldwide (Vishwakarma et al., 2016). Moreover, medium-resolution satellite data is less costly than high-resolution data.

Nowadays, machine-learning techniques on remotely sensed images for LULC mapping have received a lot of interest. There are different machine-learning algorithms such as random forest (R.F.), artificial neural network (ANN), support vector machine (SVM), fuzzy adaptive resonance theory-supervised predictive mapping (Fuzzy ARTMAP), spectral angle mapper (SAM), and Mahalanobis distance (M.D.) etc. The most popular mapping technique used on satellite imagery is random forest (R.F.) algorithms. It's one of the most widely used LULC classification machine learning algorithms. Talukdar et al. (2020) compared different

machine-learning algorithms and found that random forest (R.F.) is the best machine-learning LULC classifier. The objectives of this study are to assess and compare the satellite images, including Gaofen-6, Landsat-8, and Sentinel-2, for LULC classification using random forest (R.F.) algorithms in Mardan district, Pakistan.

II. Methodology

2.1 Study area.

Mardan district is located in Peshawar division, Khyber Pakhtunkhwa province, Pakistan, shown in Figure 1. Geographically, it lies between 34°12'0" N and 72°2'24" E. The valley's elevation ranges from 1000 to 2056 metres above sea level. It is bounded by Buner district, which is on the north; Swabi district on the east; Nowshehra district on the south; and Charsadda and Malakand districts on the west. The district has a total area of 1632 sq. km. According to census data, the population in 1998 was 1460100 people and that in 2020 was 3810000 people, which shows the rapid rate of urbanisation in the study area (Khan et al., 2011). The district's northern border is surrounded by hills, whereas its southern border is primarily made up of fertile plains with low hills strewn across it (Akhtar & Begum, 2009). The typical temperature in Mardan is between 20 and 30 degrees Celsius, and the relative humidity is relatively high, with a maximum humidity of 73 per cent recorded in December. Mardan receives 559 mm of rain on average (Anwar et al., 2019). The summer months are very hot. During May and June, dust storms are common at night. The months of July, August, December, and January get the most rainfall. Streams usually run from north to south. The Kabul River receives the majority of the streams.

Mardan District is one of Khyber Pakhtunkhwa Province's most economically prosperous areas. It is Khyber Pakhtunkhwa's second-largest city. Agriculture is the main source of income for the people in this area. It has one of the best irrigation systems in the world, which the British government established during its rule over the subcontinent. The major crops grown in this area are wheat, maize, tobacco, sugarcane, sugar beets, apricots, peaches, apples, plums, and pears. Along with agriculture, the Mardan district has a lot of opportunities for investors in the tourism, mining, and processing industries, as well as in the manufacturing of cars, railway engines, sugar, and other things like cigarettes, textiles, beverages, ceramics, edible oil/ghee, and soaps/shampoo, etc.
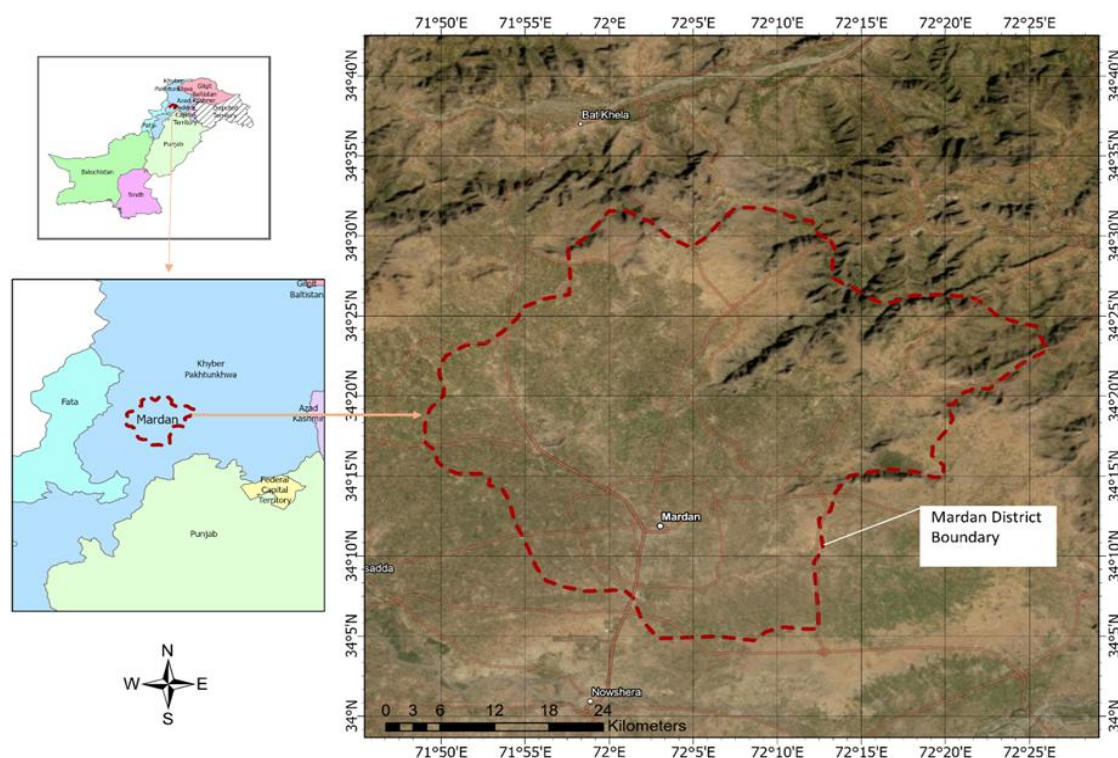

Figure 1. Study Area map of Mardan district

2.2 Data Acquisition

In order to study LULC Classification for Mardan district, images from Landsat 8 Operational Land Imager (OLI), Sentinel-2 Multispectral Instrument (MSI), and Gaofen-6 instruments were acquired from different sources. A single tile was used to cover the entire area of Mardan for Landsat-8 in January 2021. The cloud cover in the image was 3%. For sentinel-2, two tiles were used to cover the entire study area for January

2021. The cloud cover of the Sentinel-2 image was 3%. Both Landsat-8 and Sentinel-2 images were acquired from the United States Geological Survey website (earthexplorer.usgs.gov). For Gaofen-6, a single tile was used to cover the entire study area for January 2021. The Geofen-6 satellite image was taken freely from the CNSA GEO website (cnsageo.com). The satellite data acquisition information for each instrument is given in table 1. Characteristics of Landsat-8 Operational Land Imager (OLI) images for the study area

Data	Image Acquisition Date	SpatialResolution	Path/Row	CloudsPercentage	Sensor
Landsat 8 OLI	01-01-2021 to 01-02-2021	30 m	151/36	3%	OLI
Sentinel-2 MSI	01-01-2021 to 01-02-2021	10 m	43SBU & 43SBT	3%	MSI
Gaofen-6	01-01-2021 to 01-02-2021	16m		3%	WFV

2.2.1 Instruments details and background
Landsat-8

Landsat-8 is the most current in a long line of global remote sensing satellites that began in 1972 (Knight & Kvaran, 2014). Most importantly, it can monitor the Earth at wavelengths that allow researchers to correct for distortions, particularly near the coast, generated by the atmosphere (Acharya & Yang, 2015b). The two sensors of the Landsat 8 satellite are the Landsat 8 OLI and the Thermal Infrared Sensor (TIRS). There are eight spectral bands with a 30 m spatial resolution for bands 1–7 and 9, and one panchromatic band with a 15 m resolution in the Landsat 8 OLI data. The band characteristics of Landsat-8 are given in table 2 (Hua et al., 2017). The European Space Agency launched two Sentinel 2A and 2B satellites on June 23, 2015, and March 7, 2017, respectively. Two satellites are in a similar orbit and share identical characteristics. The S2/MSI mission gives additional mapping opportunities due to their spectral characteristics (three bands in the Red-edge and two bands in the SWIR). Because this spectral range is sensitive to chlorophyll concentration and extremely changeable among different crops and phenological phases, Descriptions for different bands used for Sentinel-2 are given in table 3. On June 2, 2018, China launched Gaofen-6, a new high-resolution remote sensing satellite from the Jiuquan Satellite Launch Center. Gaofen-6 is an optical satellite featuring one 2/8m Panchromatic and Multispectral imager and one 16m Wide Field of View Multispectral Camera. The band details of Gaofen-6 are shown in Table 4. The Gaofen-6 introduces four bands with core wavelengths of 710 nm, 750 nm, 425 nm, and 610 nm, which can provide more detailed spectrum data for agricultural research (Xu, 2019).

Table 2. Landsat-8 band characteristics

Sensor	Band Number	Band name	Wavelength (μm)	Resolution (m)	Band Applications
OLI	1	Coastal/ Aerosol	0.435 - 0.451	30	Coastal and aerosol studies
OLI	2	Blue	0.452 – 0.512	30	Bathymetric mapping, distinguishing soil from vegetation, and deciduous from coniferous vegetation
OLI	3	Green	0.533 – 0.590	30	Emphasizes peak vegetation, which is useful for assessing plant vigour
OLI	4	Red	0.636 – 0.673	30	Discriminates vegetation slopes
OLI	5	NIR	0.851 – 0.879	30	Emphasizes biomass content and shorelines
OLI	6	SWIR 1	1.566 – 1.651	30	Discriminates moisture content of soil and vegetation; penetrates thin clouds
OLI	7	SWIR 2	2.107 – 2.294	30	Improved ability to track moisture content of soil and vegetation and thin cloud penetration
OLI	8	Pan	0.503 – 0.676	15	15 meter resolution, sharper image definition
OLI	9	Cirrus	1.363 – 1.384	30	Improved detection of cirrus cloud contamination
TIRS	10	TIRS 1	10.6 – 11.19	100	The 100-meter resolution, thermal mapping and estimated soil moisture
TIRS	11	TIRS 2	11.50– 12.51	100	The 100-meter resolution, thermal mapping and estimated soil moisture

Sources: (eos.com/find-satellite/landsat-8/)

Table 3. Sentinel-2 band characteristics.

Sentinel-2 Bands	Central Wavelength (μm)	Resolution (m)
Band 1 - Coastal aerosol	0.443	60
Band 2 - Blue	0.490	10
Band 3 - Green	0.560	10

Band 4 - Red	0.665	10
Band 5 - Vegetation Red Edge	0.705	20
Band 6 - Vegetation Red Edge	0.740	20
Band 7 - Vegetation Red Edge	0.783	20
Band 8 - NIR	0.842	10
Band 8A - Vegetation Red Edge	0.865	20
Band 9 - Water vapors	0.945	60
Band 10 - SWIR - Cirrus	1.375	60
Band 11 - SWIR	1.610	20
Band 12 - SWIR	2.190	20

(Source: sentinels.copernicus.eu/web/sentinel/technical-guides/sentinel-2-msi/msi-instrument)

Table 4. Gaofen-6 band characteristics

Payload	Spectral	Spectral Type	Spectral Range (nm)	Resolution Spatial (m)
PMS	1	Panchromatic	450~900	2
PMS	2	Blue	450~520	8
PMS	3	Green	520~590	8
PMS	4	Red	630~690	8
PMS	5	Near infrared	770~890	8
WFV	1	Blue	450~520	16
WFV	2	Green	520~590	16
WFV	3	Red	630~690	16
WFV	4	Near infrared	770~890	16
WFV	5	Costal	400~45	16
WFV	6	Yellow	590~630	16
WFV	7	RedEdge1	690~730	16
WFV	8	RedEdge2	730~770	16

(Source: catalyst.earth/catalyst-system-files/help/references/gdb_r/Gaofen-6)
Different techniques were used to build land cover maps from these data utilising random forests (RF) algorithms after receiving Landsat-8 and Sentinel-2 data, as well as Gaofen-6 data. The results of this study are shown by the flow chart in Figure 2.
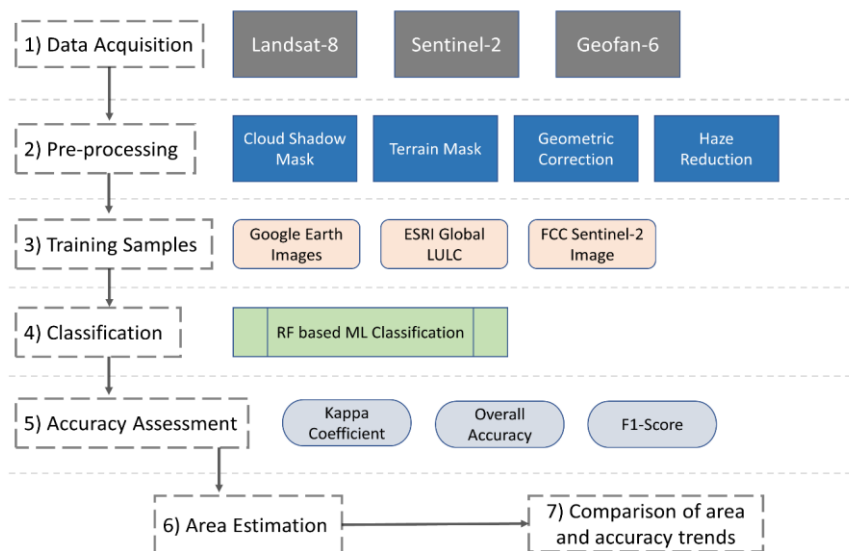

Figure2. The methodology flowchart for this study

Firstly, Landsat-8, Sentinel-2, and Gaofen-6 satellite images were collected free from different websites. Afterwards, those satellite images were corrected by atmospheric correction, cloud shadow mask, terrain mask, geometric correction, and haze reduction. Then the training samples were created carefully to depict the following five classes: water, agricultural land, bare soil, vegetation, and built-up areas. The reference data received from Google Earth Images, ESRI Global LULC, and (False Color Composite) FCC Sentinel-2 Images was used to develop training sites for each class. For this study (Topalolu et al., 2016b), Google Earth has satellite images with a high geographic and temporal resolution that were suitable for use as a reference. At least 40 samples were gathered for each land cover/use class, totaling 3400 samples for the categorization of both pictures in ArcGIS Pro. Next, random forest (RF) approaches were applied to classify land cover maps of the study area. Finally, an error matrix was used to assess accuracy. From the error matrix, accuracy assessment indices such as Kappa, Overall Accuracy (OA), User Accuracy (UA), Producer Accuracy (PA), and F1-Score were evaluated.

2.3   Pre- processing
2.3.1   Atmospheric correction

Atmospheric correction is done for each satellite image to remove the atmosphere's scattering and absorption effects. There are various methods for atmospheric correction, including dark object subtraction, radiative transfer models, and atmospheric modelling. We used the Dark Object Subtraction (DOS) method for atmospheric correction. The goal of atmospheric correction is to eliminate atmospheric effects from satellite photos in order to establish accurate surface reflectance values. The most crucial aspect of the preprocessing of satellite remotely sensed data is atmospheric correction, and any omission leads to incorrect results (Themistocleous&Hadjimitsis, 2008).

2.4   Machine Learning RF classification

There are various machine-learning algorithms for LULC mapping. Machine-learning approaches have been classified into two categories: supervised and unsupervised (Wulder et al., 2019; See et al., 2015). Spectral angle mappers include spectral angle mappers (SAM), support vector machine (SVM), fuzzy adaptive resonance theory-supervised predictive mapping (Fuzzy ARTMAP), random forest (RF), Mahalanobis distance (MD), radial basis function (RBF), decision tree (DT), maximum likelihood classifier (MLC), fuzzy logic, naive Bayes (NB), and multilayer perception (MLP) (Ma et al., 2019; Shih et al., 2019). On the other hand, unsupervised algorithms include K-means, ISODATA, Affinity Propagation (AP) cluster algorithms, etc. (Maxwell et al., 2018; Camps-Valls et al., 2011). During the last ten years, random forests (RF), artificial neural networks (ANN), support vector machines (SVM), and decision trees have received considerable attention among remote sensing communities in remote sensing-based activities like LULC classification (Talukdar et al., 2020).

2.4.1   Random forests (RF)

RF is a non-parametric ensemble learning approach that is based on the premise that a group of bootstrapped aggregated classifiers outperforms a single classifier. Every single tree is parameterized using just a randomly sampled set of observations, with substitution from the training data. This decreases multicollinearity by helping to de-correlate the trees (Abdi, 2020). Two factors are required to set up the RF model, which is referred to as the method's base. These factors are 1) the number of trees, which 'n-tree' can explain, and 2) the number of features in each split, which'm-try' can explain. Individual voting power or votes is provided by classification trees, which provide correct classification in managing the majority vote from trees across the forest (Talukdar et al., 2020). Above the bootstrapping strategy, this method uses random binary trees to build a training subset. Furthermore, a random selection of the training information is used to generate the model from the initial database; however, data that is not involved is known as "out-of-the-bag" (OOB) (Catani et al., 2013). The working of RF is shown in figure 3.
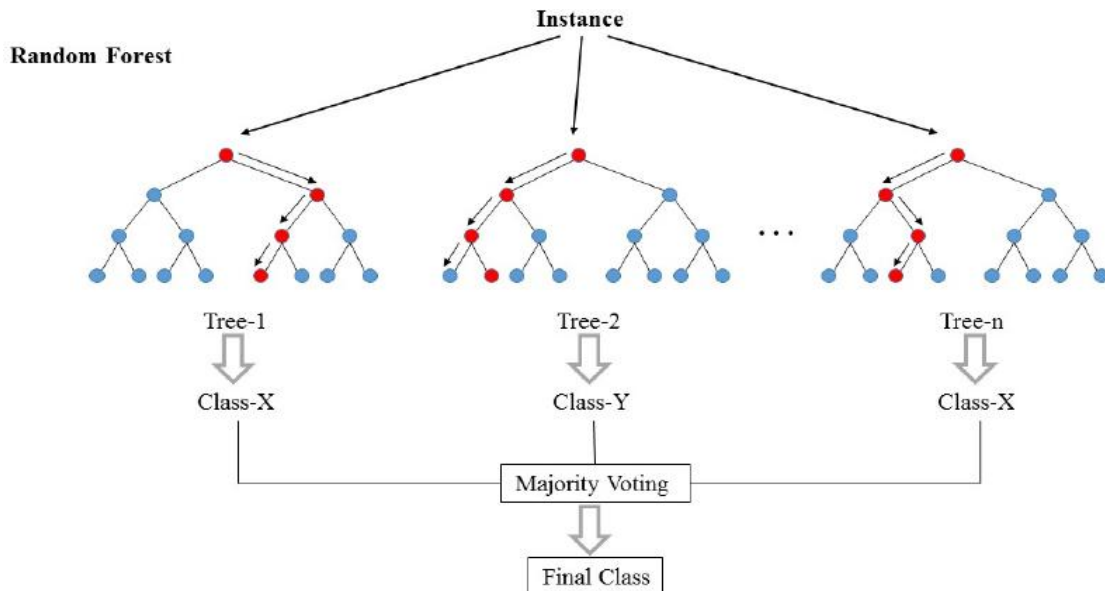
Figure 3: Random Forest algorithm working flowchart

The Random Forest (RF) approaches have been used to solve various environmental issues, including water resource management and natural disaster mitigation. It can process a wide range of data, including satellite images and numerical data. Several studies in the realm of remote-sensing applications have recently revealed that LULC classification utilising RF has reasonable performance. This method uses a large number of trees to improve accuracy in picture recognition and land-use modelling (Talukdar et al., 2020). It has attracted the attention of the scientific community due to its impressive classification findings and processing speed (Belgiu & Drăguţ, 2016). The RF methodology has benefited from two more powerful algorithms: bagging and random, which are referred to as the method's "powerhouse (Talukdar et al., 2020).

2.5   Accuracy Assessment
        Accuracy assessment is a crucial final stage in the categorization process (Rwanga & Ndambuki, 2017). It is required for the examination of the classification process result since the user of land-cover output must know how precise the result is in order to effectively use the data (Mohajane et al., 2018). In this work, we used the kappa coefficient, overall accuracy (OA), and F1 score.In accuracy evaluations, Kappa analysis is a discontinuous multivariate technique. The Khat statistic (an estimate of Kappa) is a way of measuring agreement or correctness derived from Kappa analysis.
Kappa was calculated using the following Equation:

$$K = \frac{observed\ accuracy - chance\ agreement}{1 - chance\ agreement}$$

The likelihood that a test will correctly classify an individual is defined as the sum of true positives and true negatives divided by the total number of individuals examined (Alberg et al., 2004). Overall accuracy is calculated using the following formula:
The overall classification accuracy is calculated by dividing the number of correct points by the total number of points.
        The F1-score is a metric for how accurate a model is on a given dataset. It's used to assess binary classification systems that divide examples into "positive" and "negative" categories. The F-score, which is defined as the harmonic mean of the model's precision and recall, is a technique for combining the model's precision and recall. The F-score is a popular way to judge information retrieval systems like search engines and a number of machine learning models, especially those that deal with natural language processing. The F1 measure is now widely employed in most machine learning applications, not just in binary circumstances but also in multiclass cases (Chicco & Jurman, 2020). The F1-score is calculated using the following formula:
.

$$F1 = 2 \times \frac{precision \ \times recall}{precision + recall}$$

2.6   Area Estimation
For estimating area, the per-pixel area-based approach as mentioned in was used. According to the Pixel-based area estimation approach, the area of any classified raster can be evaluated by using the following formula:

$:Area\ (ha) = \frac{x^2 \times y}{10000}$

Where x is the spatial resolution of specific satellite image, and y is the total number of pixels.

III. Results

3.1 Land-use classification using multispectral instruments

The three instruments, namely Landsat-8, Sentinel-2, and Gaofen-6, were used separately using the same training points obtained through the field survey as mentioned in the methodology section. The derived LULC maps of each instrument are shown in figures 4-6 and 7-8. Figure 4 shows the derived LULC of the Sentinel-2 MSI instrument, which shows great visuals, especially when highlighting urban areas. Figure 5 depicts LULC in the Mardan district using Gaofen-6, which shows good urban areas classified similarly to Sentinel-2, as well as perfectly differentiated forestland in the district's north eastern corner. 6 shows the derived LULC using the Landsat-8 OLI instrument at 30m resolution. Being a moderate resolution multispectral instrument, Landsaat-8 did not differentiate waterbodies along the city, but nether water channels were highlighted. The detailed visual comparison is given in the discussion section hereafter. To further investigate slight visual changes, we prepared insect maps, which are shown in figure 7.
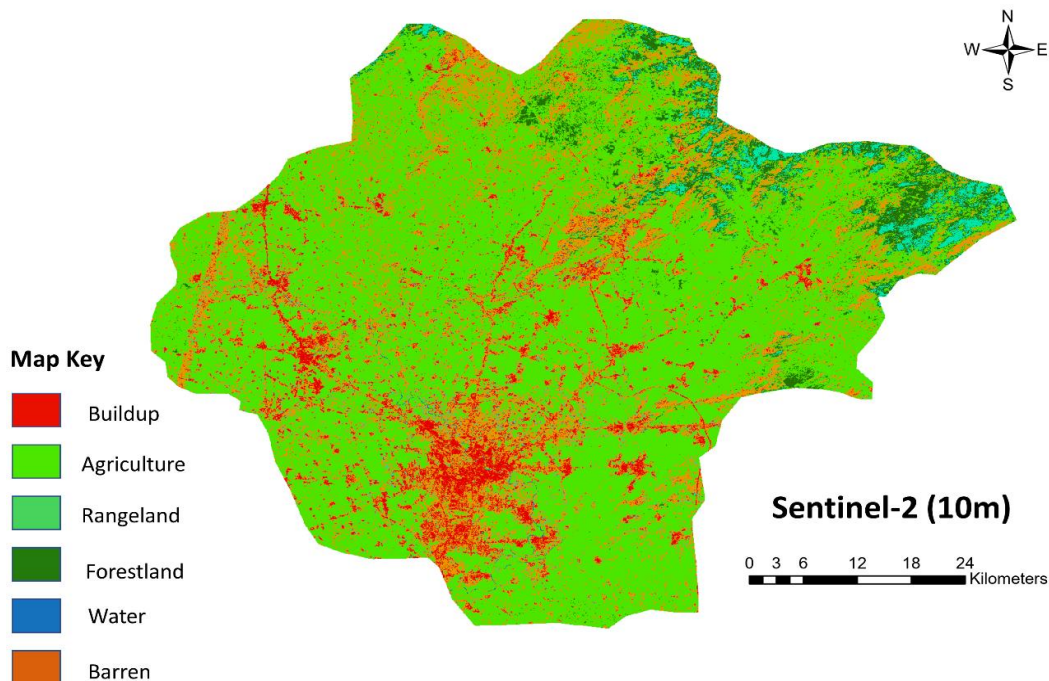

Figure 4. LULC classified map of Mardan district using Sentinel-2 at 10m resolution.
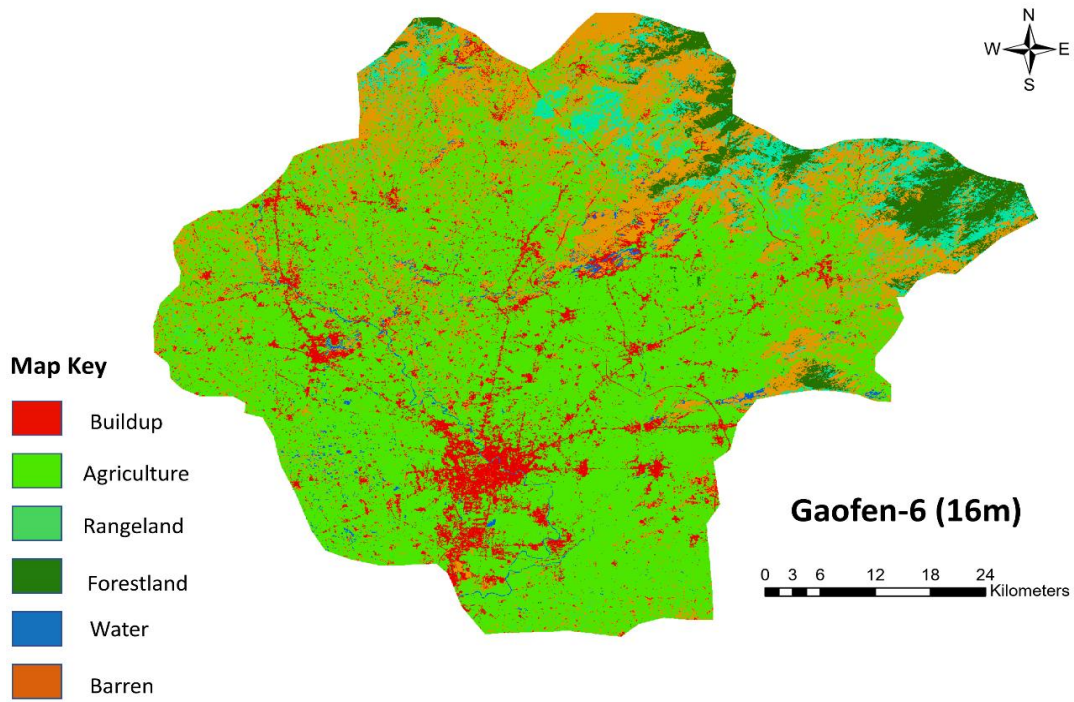
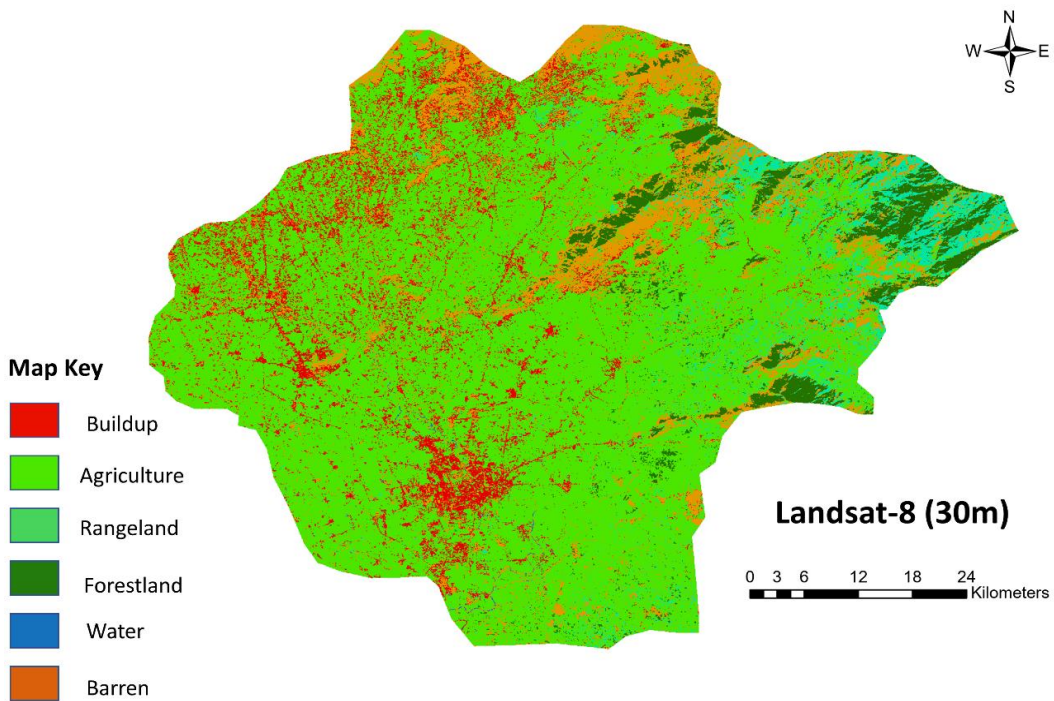Figure 5. LULC classified map of Mardan district using Gaofen-6 at 16m resolution.

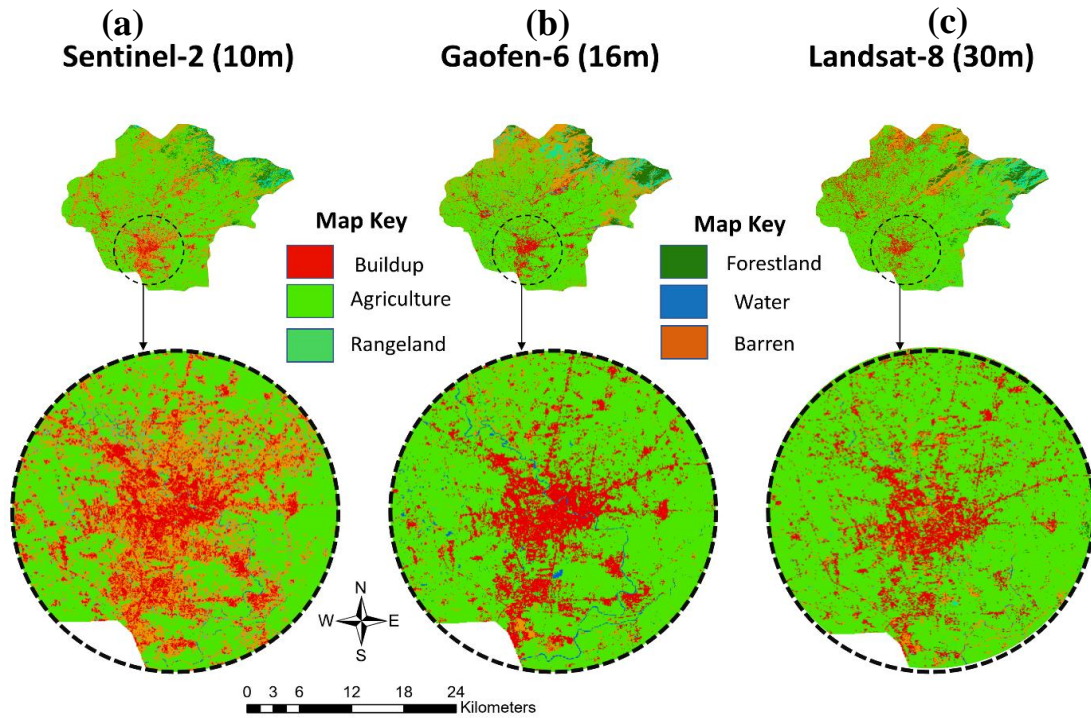Figure 6. LULC classified map of Mardan district using Landsat-8 at 30m resolution.

Figure 7. Insect maps zoomed over Mardan city to show difference in urban classified area using Sentinel-2 (a), Gaofen-6 (b) and Landsat-8 (c).

3.2 Accuracy Assessment

After obtaining LULC from each instrument, their accuracy assessment was performed. The accuracy assessment was done using validation points (30%) separated earlier as aforementioned in the methodology section. For evaluating very minute details in the accuracy of each instrument, accuracy indices including OA, K, UA, PA, and F1-score were used. The derived accuracy in statistical form is shown in table 5-7. It can be seen that in terms of accuracy, Sentinel-2 performance (OA = 0.89, K = 0.85) was better than Gaofen-6 and Landsat-8, whereas Landsat-8 stood at last with the least accuracy (OA = 0.76, K = 0.70).

Table 5. Accuracy assessment of derived LULC maps from Sentinel-2

Sentinel-2					
	OA	K	UA	PA	F1s
Buildup	0.89	0.85	0.83	0.86	0.84
Agriculture			0.86	0.86	0.86
Rangeland			0.85	0.86	0.85
Forestland			0.86	0.8	0.86
Water			0.91	0.89	0.92
Barren			0.85	0.78	0.82

Table 6. Accuracy assessment of derived LULC maps from Gaofen-6

Gaofen-6					
	OA	K	UA	PA	F1s
Buildup	0.80	0.79	0.79	0.77	0.8
Agriculture			0.8	0.72	0.77
Rangeland			0.79	0.86	0.81
Forestland			0.77	0.71	0.74
Water			0.9	0.87	0.88
Barren			0.88	0.81	0.82

Table 7. Accuracy assessment of derived LULC maps from Landsat-8

Landsat-8					
	OA	K	UA	PA	F1s
Buildup	0.76	0.70	0.63	0.66	0.64
Agriculture			0.73	0.76	0.71
Rangeland			0.72	0.73	0.72
Forestland			0.73	0.67	0.73
Water			0.74	0.74	0.74
Barren			0.72	0.65	0.69

3.3 Area Estimation

For estimating area, we used a pixel-based approach as mentioned in the methodology section earlier. The percentage area for each instrument in the form of a pie-chart is shown in figure 8-10. From figures 8–10, it was noticed that the least urban area was calculated by Sentinel-2 (figure 8), whereas the highest vegetation area was demonstrated by Landsat-8 (figure 10).
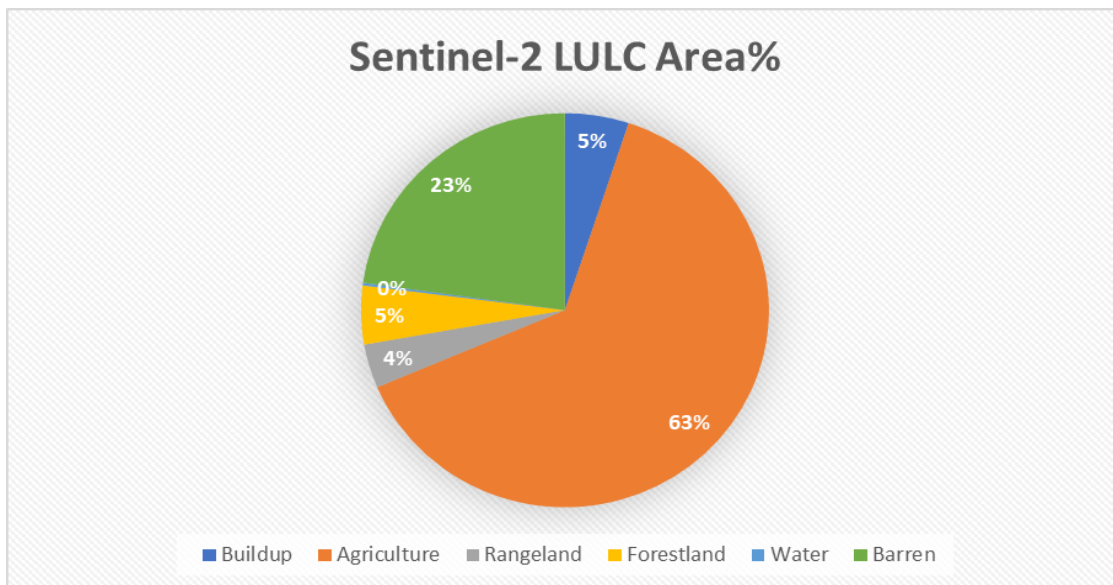

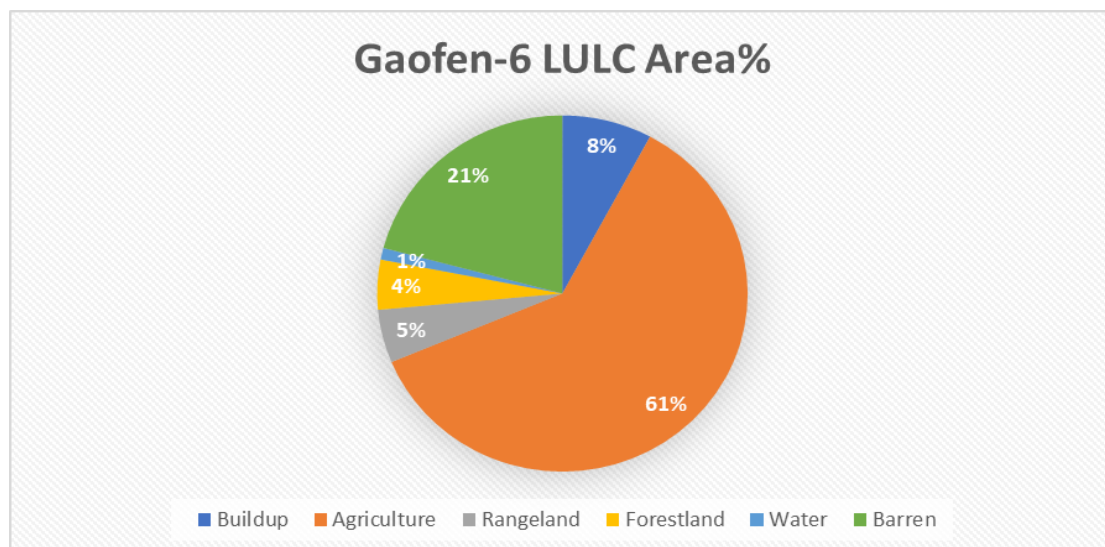Figure 8. Pie-Chart showing area percentage distribution of LULC derived from Sentinel-2

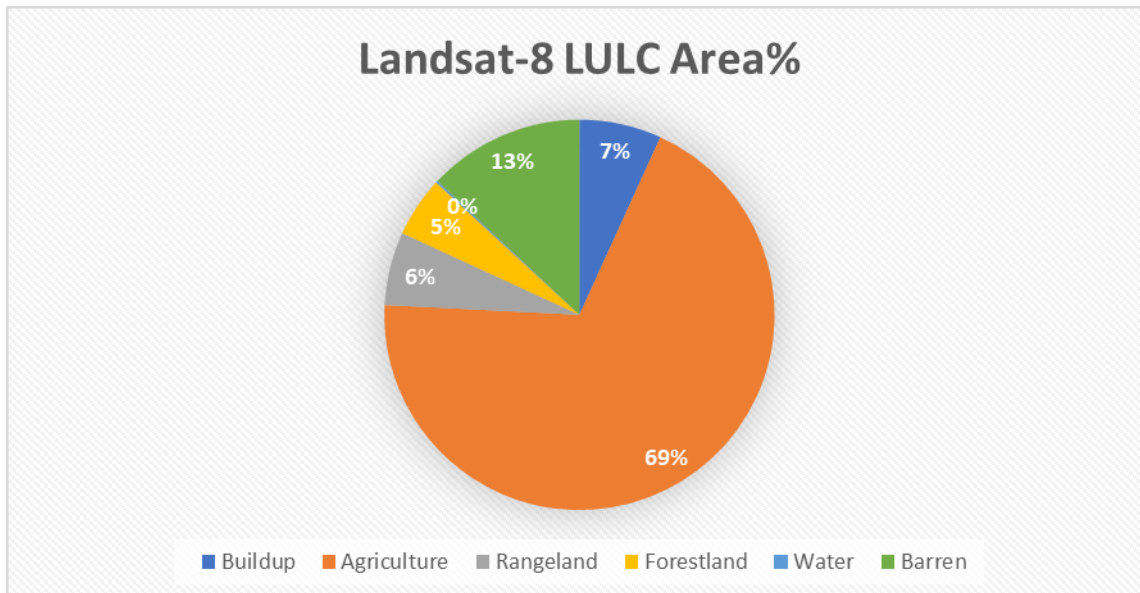Figure 9. Pie-Chart showing area percentage distribution of LULC derived from Gaofen-6

Figure 10. Pie-Chart showing area percentage distribution of LULC derived from Landsat-8

To evaluate the comparison between areas estimated from different instruments, we compared the areas in hectares using a bar chart. The resulting bar chart showing variations in area (ha) is shown in figure 11. The bar chart further highlighted that water area was the maximum shown by the Gaofen-6 instrument, whereas the least urban area was shown by Sentinel-2. Another point highlighted by figure 11 is that when observing areas of barren class, the Sentinel-2 and Gaofen-6 show similar results, whereas Landsat-8 shows a lower area.
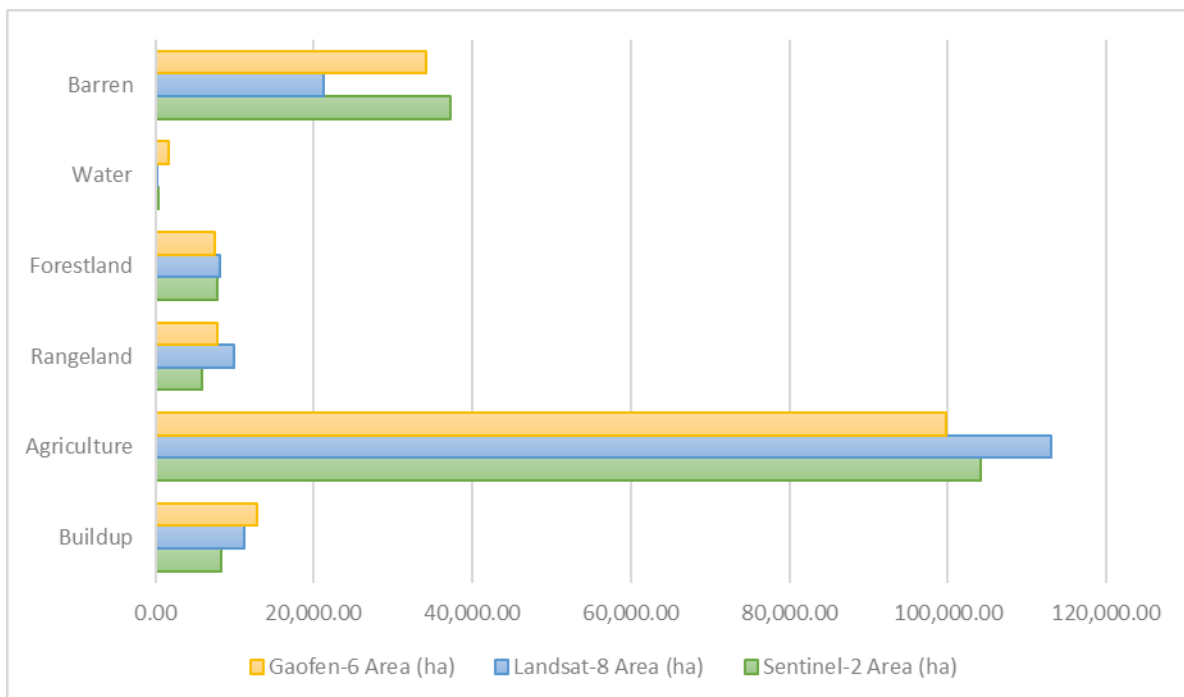

Figure11. Bar chart showing area distribution (ha) of LULC derived from Sentinel-2, Gaofen-6 and Landsat-8.

IV. Discussion

This study compared the efficiency of three multispectral instruments, namely Sentinel-2, Gaofen-6, and Landsat-8, in land use classification over Mardan district, Pakistan. The results from land-use maps show strange trends. Figure 4 shows the derived LULC map using the Sentinel-2 MSI instrument at 10m spatial resolution. On critically observing, it was found that it precisely differentiated the urban areas from the adjoining barren or uncultivated land. For example, in the central city region (Mardan City), the urban area looks well classified when seen with an overlay over a base map. Another point considered when looking at

figure 4 was the classification of forest areas in the north-eastern part of the district. When compared to the actual base map, Sentinel-2 classified only high-density forest areas, while nearby forest areas with less than 30% forest cover were classified as rangelands or agriculture.Apart from this, some deviation was also observed visually in Figure 4, like the neighbouring urban areas alongside the central city area were shown as barren, whereas in reality they were urban.

Figure 5 shows LULC classification using the Gaofen-6 instrument. On critical observation, it was observed that Gaofen-6 very efficiently differentiates water bodies. Even small ice caps on mountain peaks were properly classified as water (which were not identified using Sentinel-2 and Landsa-8). Furthermore, Gaofen-6 has successfully differentiated adjoining buildup areas. A slight discrimination was observed between the barren and agriculture/rangeland classes. Some areas on the north side of the district were also falsely classified. On further observation, perennial grassland on the northern side of the district was mostly classified as barren as Gaofen-6 was not able to differentiate properly there.

The last LULC derived map of Mardan district using Landsat-8 is shown in figure 6. On critically observing the map and comparing the map against the base map, the only good classified classes were forest, core-urban, and agriculture. It was observed that Landsat-8 had classified any dense forest area with 30% forest cover. The downside of Landsat-8 was that it does not efficiently differentiate urban areas, especially those adjoining towns, infrastructures, and roads. Another issue observed in Landsat-8 was that water channels were misclassified as urban areas and only water bodies with coverage greater than 40% were properly classified.

To further investigate slight visual changes, we prepared insect maps, which are shown in figure 7. Figures (4-6) confirm our previous deductions from the insect map focused on Mardan city.In Figure 7b, the Gaofen-6 shows promising outcomes, especially when differentiating urban land. It also has an advantage over Sentinel-2 (figure 7a) and Landsat-8 (figure 7c) that it properly delineates urban land with adjoining agricultural land, such as open land. In a contest, Sentinel-2 and Landsat-8 misclassified nearby areas as barren and agricultural, respectively. Lastly, another thing noticed in Landsat-8 was the Urban Green Space (UGS) misclassification. UGS are the inter-city greenery that promotes sustainability and reduces the effect of global warming. Unfortunately, Landsat-8-derived LULC shows the majority of adjacent urban land as agriculture (i.e., UGS), despite the fact that there was only a small fraction of UGS present (less than 20%).

Moving forward to the accuracy assessment, the accuracy assessment gives new insights towards the efficiency of derived land use and land cover maps. Table 5-7 shows the accuracy statistics of Sentinel-2, Gaofen-6, and Landsat-8 and reveals that Sentinel-2 was the best performing instrument while Landsat-8 was the least in performance. The OA and K statistics of Sentinel-2 were far better than those of Gaofen-6 and Landsat-8. To conclude, table 5-7 depicts the distribution of individual class accuracy and reveals that specific class accuracies were similar in the cases of Sentinel-2 and Gaofen-6, but for Landsat-8, the accuracies of LULC classes were abrupt.

For evaluating the efficiency of multispectral instruments, we used estimated areas and compared the results. The pie charts (figure 8-10) show the percentage distribution of the estimated area of different LULC classes of each instrument. On visual observing the charts, it showed that both three instruments have similar area distribution, i.e., the highest area percentage was agriculture (61-69%), then barren (13-23%), and at third, buildup area (5-8%). The pie charts also showed that the least class having the lowest area percentage was water (1%).

To further investigate the intercomparison of area (ha) statistics of different classes per instrument, we prepared the bar chart shown in figure 11. The bar chart shows the detailed comparison of each land-use class, which further reveals that there are some prominent differences, which are discussed hereafter. Landsat-8 has overestimated the agricultural area, whereas, on the other hand, it has the least area of barren land. On visual observing the figure 7 earlier, it also confirmed that the barren area was prominently misclassified alongside the city of Mardan in the case of Sentinel-2, while Gaofen-6 accurately showed some nearby areas as urban or as vegetation. These instruments (Sentinel-2, and Gaofen-6) were still successful in differentiating the dense city boundary, while on the other hand, Landsat-8 only categorised dense impervious surfaces as buildup while the rest were categorised as agriculture (due to the presence of UGS). This gives rise to a high agriculture area, whereas the least barren and the second least built up area. Another aspect that was confirmed from Figure 7 as compared with Figure 11 was the distribution of buildup area in the case of Gaofen-6. As mentioned earlier, Gaofen-6 differentiated very efficiently the buildup areas, while in the case of Sentinel-2, the nearby impervious surfaces were misclassified as barren, and that's why Sentinel-2 showed the highest barren area than others, which was also confirmed through figure 7. In the case of Sentinel-2, the misclassification of barren land near Mardan city was mostly due to similar spectral characteristics of builtup and barren land as discussed by Attri et al. (2015). Due to this, the Sentinel-2 also misclassified some nearby urban and shrubland as barren (figure 10). On August 1, 2010, this entry was published.

V. Conclusion

This study evaluated the comparison of Sentinel-2, Gaofen-6, and Landsat-8 in land-use classification over Mardan, Pakistan. The results of this study revealed three important findings. Firstly, the Sentinel-2 instrument has the best accuracy results compared to Gaofen-6 and Landsat-8, but for specific classes of buildup and barren classes, Sentinel-2 showed misclassification. Visually, it was observed that Sentinel-2 has misclassified some nearby urban areas as barren land despite being urban, while Gaofen-6 has classified the urban area perfectly. Secondly, Landsat-8 accuracy and area results showed that the performance of this instrument was the lowest compared to Sentinel-2 and Gaofen-6. While Landsat-8 performed well while classifying rangeland and forestland with reasonable accuracy, it wasn't enough to properly differentiate urban areas and only classified dense impervious surfaces as buildup. Lastly, Gaofen-6 performance was much better in terms of differentiating urban areas with nearby shrubland and for differentiating intercity wetlands and waterbodies. The findings of this study will provide new insights into the proper application of various multispectral instruments for specific tasks in which they excelled. Future research should focus on the detailed comparison of active and passive satellite instruments in classifying land-use and land-cover.

Acknowledgement

Reference

[1]. Abd El-Ghani, M. M., Huerta-Martínez, F. M., Hongyan, L., & Qureshi, R. (2017). The deserts of Pakistan. In *Plant Responses to Hyperarid Desert Environments* (pp. 547–573). Springer.

[2]. Abdi, A. M. (2020). Land cover and land use classification performance of machine learning algorithms in a boreal landscape using Sentinel-2 data. *GIScience& Remote Sensing*, *57*(1), 1–20.

[3]. Acharya, T. D., & Yang, I. (2015a). Exploring landsat 8. *International Journal of IT, Engineering and Applied Sciences Research (IJIEASR)*, *4*(4), 4–10.

[4]. Acharya, T. D., & Yang, I. (2015b). Exploring landsat 8. *International Journal of IT, Engineering and Applied Sciences Research (IJIEASR)*, *4*(4), 4–10.

[5]. Ahmad, S., & Islam, M. (2011). Rangeland productivity and improvement potential in highlands of Balochistan, Pakistan. *Biomass-Detection, Production and Usage. In-Tech, Rijeka, Croatia*, 289–304.

[6]. Akhtar, N., & Begum, S. (2009). Ethnopharmacological important plants of Jalala, district Mardan, Pakistan. *Pak. J. Pl. Sci*, *15*(2), 95–100.

[7]. Alberg, A. J., Park, J. W., Hager, B. W., Brock, M. v, & Diener-West, M. (2004). The use of "overall accuracy" to evaluate the validity of screening or diagnostic tests. *Journal of General Internal Medicine*, *19*(5p1), 460–465.

[8]. Al-Doski, J., Mansor, S. B., &Khuzaimah, Z. (2020). Improved Land Cover Mapping Using Landsat 8 Thermal Imagery. *IOP Conference Series: Earth and Environmental Science*, *540*(1), 012022.

[9]. Anderson, J. R. (1976). *A land use and land cover classification system for use with remote sensor data* (Vol. 964). US Government Printing Office.

[10]. Anwar, F., Ahmad, S., Haroon, M., Haq, I. U., Khan, H. U., Khan, J., & Shah, I. A. (2019). Dengue virus epidemics: A recent report of 2017 from district Mardan, Khyber Pakhtunkhwa province, Pakistan. *International Journal of Mosquito Research*, *6*(1), 46–49.

[11]. Arowolo, A. O., Deng, X., Olatunji, O. A., &Obayelu, A. E. (2018). Assessing changes in the value of ecosystem services in response to land-use/land-cover dynamics in Nigeria. *Science of the Total Environment*, *636*, 597–609.

[12]. Belgiu, M., &Drăguţ, L. (2016). Random forest in remote sensing: A review of applications and future directions. *ISPRS Journal of Photogrammetry and Remote Sensing*, *114*, 24–31.

[13]. Bruzzone, L., Bovolo, F., Paris, C., Solano-Correa, Y. T., Zanetti, M., & Fernández-Prieto, D. (2017). Analysis of multitemporal Sentinel-2 images in the framework of the ESA Scientific Exploitation of Operational Missions. *2017 9th International Workshop on the Analysis of Multitemporal Remote Sensing Images (MultiTemp)*, 1–4.

[14]. Cai, G., Ren, H., Yang, L., Zhang, N., Du, M., & Wu, C. (2019). Detailed urban land use land cover classification at the metropolitan scale using a three-layer classification scheme. *Sensors*, *19*(14), 3120.

[15]. Camps-Valls, G., Benediktsson, J. A., Bruzzone, L., &Chanussot, J. (2011). Introduction to the issue on advances in remote sensing image processing. *IEEE Journal of Selected Topics in Signal Processing*, *5*(3), 365–369.

[16]. Catani, F., Lagomarsino, D., Segoni, S., &Tofani, V. (2013). Landslide susceptibility estimation by random forests technique: sensitivity and scaling issues. *Natural Hazards and Earth System Sciences*, *13*(11), 2815–2831.

[17]. Cazaubiel, V., Chorvalli, V., &Miesch, C. (2017). The multispectral instrument of the Sentinel2 program. *International Conference on Space Optics—ICSO 2008*, *10566*, 105660H.

[18]. Chen, B., Xu, B., & Gong, P. (2021). Mapping essential urban land use categories (EULUC) using geospatial big data: Progress, challenges, and opportunities. *Big Earth Data*, *5*(3), 410–441.

[19]. Chicco, D., &Jurman, G. (2020). The advantages of the Matthews correlation coefficient (MCC) over F1 score and accuracy in binary classification evaluation. *BMC Genomics*, *21*(1), 1–13.

[20]. Coulston, J. W., Reams, G. A., Wear, D. N., & Brewer, C. K. (2014). An analysis of forest land use, forest land cover and change at policy-relevant scales. *Forestry*, *87*(2), 267–276.

[21]. Dhanaraj, K., & Angadi, D. P. (2020). Land use land cover mapping and monitoring urban growth using remote sensing and GIS techniques in Mangaluru, India. *GeoJournal*, 1–27.

[22]. Doyle, C., Beach, T., &Luzzadder-Beach, S. (2021). Tropical Forest and Wetland Losses and the Role of Protected Areas in Northwestern Belize, Revealed from Landsat and Machine Learning. *Remote Sensing*, *13*(3), 379.

[23]. Dutta, D., Rahman, A., Paul, S. K., & Kundu, A. (2019). Changing pattern of urban landscape and its effect on land surface temperature in and around Delhi. *Environmental Monitoring and Assessment*, *191*(9), 1–15.

[24]. Dutta, D., Rahman, A., Paul, S. K., & Kundu, A. (2020). Estimating urban growth in peri-urban areas and its interrelationships with built-up density using earth observation datasets. *The Annals of Regional Science*, *65*(1), 67–82.

[25]. ED Chaves, M., CA Picoli, M., & D Sanches, I. (2020). Recent applications of Landsat 8/OLI and Sentinel-2/MSI for land use and land cover mapping: A systematic review. *Remote Sensing*, *12*(18), 3062.

[26]. (FAO), F. and A. O. (2014). *FAO statistical yearbook 2014, Asia and the Pacific, Food and Agriculture*. United Nations, Food and Agriculture Organization Bangkok, Thailand.

[27]. FRA, F. A. O. (2015). Global forest resources assessment 2015 Desk reference. *Food and Agriculture Organization of the United Nations, Rome*.

[28]. Fu, W., Ma, J., Chen, P., & Chen, F. (2020). Remote sensing satellites for digital earth. In *Manual of Digital Earth* (pp. 55–123). Springer, Singapore.

[29]. Gadrani, L., Lominadze, G., &Tsitsagi, M. (2018). F assessment of landuse/landcover (LULC) change of Tbilisi and surrounding area using remote sensing (RS) and GIS. *Annals of Agrarian Science*, *16*(2), 163–169.

[30]. Gallego, F. J. (2004). Remote sensing and land cover area estimation. *International Journal of Remote Sensing*, *25*(15), 3019–3047.

[31]. Gallego, F. J. (2007). Review of the main remote sensing methods for crop area estimates. *Workshop Proceedings: Remote Sensing Support to Crop Yield Forecast and Area Estimates*, 65–70.

[32]. Ghayour, L., Neshat, A., Paryani, S., Shahabi, H., Shirzadi, A., Chen, W., Al-Ansari, N., Geertsema, M., Pourmehdi Amiri, M., &Gholamnia, M. (2021). Performance Evaluation of Sentinel-2 and Landsat 8 OLI Data for Land Cover/Use Classification Using a Comparison between Machine Learning Algorithms. *Remote Sensing*, *13*(7), 1349.

[33]. Gudmann, A., Csikós, N., Szilassi, P., &Mucsi, L. (2020). Improvement in satellite image-based land cover classification with landscape metrics. *Remote Sensing*, *12*(21), 3580.

[34]. Güler, M., Yomralıoğlu, T., & Reis, S. (2007). Using landsat data to determine land use/land cover changes in Samsun, Turkey. *Environmental Monitoring and Assessment*, *127*(1), 155–167.

[35]. Hansen, M. C., & Loveland, T. R. (2012). A review of large area monitoring of land cover change using Landsat data. *Remote Sensing of Environment*, *122*, 66–74.

[36]. Hassan, M., Ali, K. W., Amin, F. R., Ahmad, I., Khan, M. I., & Abbas, M. (2016). Economical perspective of sustainability in agriculture and environment to achieve Pakistan vision 2025. *Int J Agric Environ Res*, *2*(2), 113–124.

[37]. Hu, T., Yang, J., Li, X., & Gong, P. (2016). Mapping urban land use by using landsat images and open social data. *Remote Sensing*, *8*(2), 151.

[38]. Hua, L., Zhang, X., Chen, X., Yin, K., & Tang, L. (2017). A feature-based approach of decision tree classification to map time series urban land use and land cover with Landsat 5 TM and Landsat 8 OLI in a Coastal City, China. *ISPRS International Journal of Geo-Information*, *6*(11), 331.

[39]. Immitzer, M., Vuolo, F., &Atzberger, C. (2016). First experience with Sentinel-2 data for crop and tree species classifications in central Europe. *Remote Sensing*, *8*(3), 166.

[40]. Khan, M., Hussain, F., &Musharaf, S. (2011). A fraction of fresh water algae of Kalpani stream and adjoining area of district Mardan, Pakistan. *International Journal of Biosciences*, *1*(3), 45–50.

[41]. Knight, E. J., &Kvaran, G. (2014). Landsat-8 operational land imager design, characterization and performance. *Remote Sensing*, *6*(11), 10286–10305.

[42]. LaGro, J. A. (2005). LAND-USE CLASSIFICATION. In D. Hillel (Ed.), *Encyclopedia of Soils in the Environment* (pp. 321–328). Elsevier. https://doi.org/https://doi.org/10.1016/B0-12-348530-4/00530-0

[43]. Lai, S.-K. (2020). Effects of land use plans on urban development: A property rights approach. *Journal of Urban Management*, *9*(1), 1–5.

[44]. Lei, G., Li, A., Bian, J., & Zhang, Z. (2020). The roles of criteria, data and classification methods in designing land cover classification systems: evidence from existing land cover data sets. *International Journal of Remote Sensing*, *41*(14), 5062–5082.

[45]. Lepers, E., Lambin, E. F., Janetos, A. C., DeFries, R., Achard, F., Ramankutty, N., & Scholes, R. J. (2005). A synthesis of information on rapid land-cover change for the period 1981–2000. *BioScience*, *55*(2), 115–124.

[46]. Lindquist, E. J., D'Annunzio, R., Gerrand, A., MacDicken, K., Achard, F., Beuchle, R., Brink, A., Eva, H. D., Mayaux, P., & San-Miguel-Ayanz, J. (2012). *Global forest land-use change 1990-2005.* (Issue 169). Food and agriculture organization of the United nations (FAO).

[47]. Lu, Y., Wu, P., Ma, X., & Li, X. (2019). Detection and prediction of land use/land cover change using spatiotemporal data fusion and the Cellular Automata–Markov model. *Environmental Monitoring and Assessment*, *191*(2), 68.

[48]. Ma, L., Liu, Y., Zhang, X., Ye, Y., Yin, G., & Johnson, B. A. (2019). Deep learning in remote sensing applications: A meta-analysis and review. *ISPRS Journal of Photogrammetry and Remote Sensing*, *152*, 166–177.

[49]. Malik, S. J., Ali, S., Riaz, K., Whitney, E., Malek, M., & Waqas, A. (2017). Agriculture, Land, and Productivity in Pakistan. In *Agriculture and the Rural Economy in Pakistan* (pp. 41–80). University of Pennsylvania Press.

[50]. Mannan, A., Liu, J., Zhongke, F., Khan, T. U., Saeed, S., Mukete, B., ChaoYong, S., Yongxiang, F., Ahmad, A., & Amir, M. (2019). Application of land-use/land cover changes in monitoring and projecting forest biomass carbon loss in Pakistan. *Global Ecology and Conservation*, *17*, e00535.

[51]. Mansoor, M., Jamil, M., Anwar, F., Awan, A. A., & Muhammad, S. (2018). Review A Review on Rangeland Management in Pakistan, Bottlenecks and Recommendations. *Biological Sciences-PJSIR*, *61*(2), 115–120.

[52]. Markham, B., Storey, J., & Morfitt, R. (2015). *Landsat-8 sensor characterization and calibration*. Multidisciplinary Digital Publishing Institute.

[53]. Maxwell, A. E., Warner, T. A., & Fang, F. (2018). Implementation of machine-learning classification in remote sensing: An applied review. *International Journal of Remote Sensing*, *39*(9), 2784–2817.

[54]. Miller, J. D., & Hutchins, M. (2017). The impacts of urbanisation and climate change on urban flooding and urban water quality: A review of the evidence concerning the United Kingdom. *Journal of Hydrology: Regional Studies*, *12*, 345–362.

[55]. Mohajane, M., Essahlaoui, A., Oudija, F., Hafyani, M. el, Hmaidi, A. el, Ouali, A. el, Randazzo, G., & Teodoro, A. C. (2018). Land use/land cover (LULC) using landsat data series (MSS, TM, ETM+ and OLI) in Azrou Forest, in the Central Middle Atlas of Morocco. *Environments*, *5*(12), 131.

[56]. Monserud, R. A., &Leemans, R. (1992). Comparing global vegetation maps with the Kappa statistic. *Ecological Modelling*, *62*(4), 275–293.

[57]. Morales-Hidalgo, D., Kleinn, C., & Scott, C. T. (2017). *Voluntary guidelines on national forest monitoring*.

[58]. Mou, H., Li, H., Zhou, Y., & Dong, R. (2021). Response of Different Band Combinations in Gaofen-6 WFV for Estimating of Regional Maize Straw Resources Based on Random Forest Classification. *Sustainability*, *13*(9), 4603.

[59]. Mridha, N., Chakraborty, D., Roy, A., & Kharia, S. K. (n.d.). *Role of Remote Sensing in Land Use and Land Cover Modelling*.

[60]. Naikoo, M. W., Rihan, M., &Ishtiaque, M. (2020). Analyses of land use land cover (LULC) change and built-up expansion in the suburb of a metropolitan city: Spatio-temporal analysis of Delhi NCR using landsat datasets. *Journal of Urban Management*, *9*(3), 347–359.

[61]. Nguyen, H. T. T., Doan, T. M., Tomppo, E., & McRoberts, R. E. (2020). Land Use/land cover mapping using multitemporal Sentinel-2 imagery and four classification methods—A case study from Dak Nong, Vietnam. *Remote Sensing*, *12*(9), 1367.

[62]. Novelli, A., Aguilar, M. A., Nemmaoui, A., Aguilar, F. J., & Tarantino, E. (2016). Performance evaluation of object based greenhouse detection from Sentinel-2 MSI and Landsat 8 OLI data: A case study from Almería (Spain). *International Journal of Applied Earth Observation and Geoinformation*, *52*, 403–411.

[63]. Pandey, P. C., Koutsias, N., Petropoulos, G. P., Srivastava, P. K., & ben Dor, E. (2021a). Land use/land cover in view of earth observation: data sources, input dimensions, and classifiers—a review of the state of the art. *Geocarto International*, *36*(9), 957–988.

[64]. Pandey, P. C., Koutsias, N., Petropoulos, G. P., Srivastava, P. K., & ben Dor, E. (2021b). Land use/land cover in view of earth observation: data sources, input dimensions, and classifiers—a review of the state of the art. *Geocarto International*, *36*(9), 957–988.

[65]. Pandey, P. C., Koutsias, N., Petropoulos, G. P., Srivastava, P. K., & ben Dor, E. (2021c). Land use/land cover in view of earth observation: data sources, input dimensions, and classifiers—a review of the state of the art. *Geocarto International*, *36*(9), 957–988.

[66]. Parece, T. E., & Campbell, J. B. (2015). Land use/land cover monitoring and geospatial technologies: An overview. *Advances in Watershed Science and Assessment*, 1–32.

[67]. Parece, T. E., Campbell, J. B., & Carroll, D. (2014). Assessing variations in urban heat island effects within Roanoke, Virginia. *American Society of Photogrammetry and Remote Sensing Annual Conference. Louisville*, 23–28.

[68]. Pervaiz, W., Uddin, V., Khan, S. A., & Khan, J. A. (2016). Satellite-based land use mapping: comparative analysis of Landsat-8, Advanced Land Imager, and big data Hyperion imagery. *Journal of Applied Remote Sensing*, *10*(2), 026004.

[69]. Phiri, D., Simwanda, M., Salekin, S., Nyirenda, V. R., Murayama, Y., &Ranagalage, M. (2020). Sentinel-2 data for land cover/use mapping: a review. *Remote Sensing*, *12*(14), 2291.

[70]. Piao, Y., Jeong, S., Park, S., & Lee, D. (2021). Analysis of Land Use and Land Cover Change Using Time-Series Data and Random Forest in North Korea. *Remote Sensing*, *13*(17), 3501.

[71]. Reddy, C. S., Saranya, K. R. L., Pasha, S. V., Satish, K. v, Jha, C. S., Diwakar, P. G., Dadhwal, V. K., Rao, P. V. N., & Murthy, Y. V. N. K. (2018). Assessment and monitoring of deforestation and forest fragmentation in South Asia since the 1930s. *Global and Planetary Change*, *161*, 132–148.

[72]. Ridwan, M. A., Radzi, N. A. M., Ahmad, W., Mustafa, I. S., Din, N. M., Jalil, Y. E., Isa, A. M., Othman, N. S., &Zaki, W. (2018). *Applications of landsat-8 data: A Survey*.

[73]. Rihan, M., Naikoo, M. W., Ali, M. A., Usmani, T. M., & Rahman, A. (2021). Urban Heat Island Dynamics in Response to Land-Use/Land-Cover Change in the Coastal City of Mumbai. *Journal of the Indian Society of Remote Sensing*, *49*(9), 2227–2247.

[74]. Ritchie, H., &Roser, M. (2021). Forests and Deforestation. *Our World in Data*.

[75]. Rwanga, S. S., &Ndambuki, J. M. (2017). Accuracy assessment of land use/land cover classification using remote sensing and GIS. *International Journal of Geosciences*, *8*(04), 611.

[76]. Saah, D., Tenneson, K., Matin, M., Uddin, K., Cutter, P., Poortinga, A., Nguyen, Q. H., Patterson, M., Johnson, G., &Markert, K. (2019). Land cover mapping in data scarce environments: challenges and opportunities. *Frontiers in Environmental Science*, *7*, 150.

[77]. Saeed, A. (2003). The underlying causes of deforestation and forest degradation in Pakistan. *The XII World Forestry Congress 2003, Quebec City, Canada*.

[78]. See, L., Fritz, S., You, L., Ramankutty, N., Herrero, M., Justice, C., Becker-Reshef, I., Thornton, P., Erb, K., & Gong, P. (2015). Improved global cropland data as an essential ingredient for food security. *Global Food Security*, *4*, 37–45.

[79]. Sekertekin, A., Marangoz, A. M., &Akcin, H. (2017). Pixel-based classification analysis of land use land cover using Sentinel-2 and Landsat-8 data. *Int. Arch. Photogramm. Remote Sens. Spat. Inf. Sci*, *42*, 91–93.

[80]. Shih, H., Stow, D. A., & Tsai, Y. H. (2019). Guidance on and comparison of machine learning classifiers for Landsat-based land cover and land use mapping. *International Journal of Remote Sensing*, *40*(4), 1248–1274.

[81]. Sleeter, B. M., Wilson, T. S., Sharygin, E., &Sherba, J. T. (2017). Future scenarios of land change based on empirical data and demographic trends. *Earth's Future*, *5*(11), 1068–1083.

[82]. Sohl, T. L., Wimberly, M. C., Radeloff, V. C., Theobald, D. M., &Sleeter, B. M. (2016). Divergent projections of future land use in the United States arising from different models and scenarios. *Ecological Modelling*, *337*, 281–297.

[83]. Talukdar, S., Singha, P., Mahato, S., Pal, S., Liou, Y.-A., & Rahman, A. (2020). Land-use land-cover classification by machine learning classifiers for satellite observations—a review. *Remote Sensing*, *12*(7), 1135.

[84]. Tariq, M., & Aziz, R. (2015). An overview of deforestation causes and its environmental hazards in khyberpukhtunkhwa. *Journal of Natural Sciences Research*, *5*(1), 52–58.

[85]. Themistocleous, K., &Hadjimitsis, D. (2008). *The importance of considering atmospheric correction in the pre-processing of satellite remote sensing data intended for the management and detection of cultural sites: a case study of the Cyprus area*.

[86]. Tong, X., Zhao, W., Xing, J., & Fu, W. (2016). Status and development of china high-resolution earth observation system and application. *2016 IEEE International Geoscience and Remote Sensing Symposium (IGARSS)*, 3738–3741.

[87]. Topaloğlu, R. H., Sertel, E., &Musaoğlu, N. (2016a). ASSESSMENT OF CLASSIFICATION ACCURACIES OF SENTINEL-2 AND LANDSAT-8 DATA FOR LAND COVER/USE MAPPING. *International Archives of the Photogrammetry, Remote Sensing & Spatial Information Sciences*, *41*.

[88]. Topaloğlu, R. H., Sertel, E., &Musaoğlu, N. (2016b). ASSESSMENT OF CLASSIFICATION ACCURACIES OF SENTINEL-2 AND LANDSAT-8 DATA FOR LAND COVER/USE MAPPING. *International Archives of the Photogrammetry, Remote Sensing & Spatial Information Sciences*, *41*.

[89]. Turner, B., Meyer, W. B., & Skole, D. L. (1994). Global land-use/land-cover change: towards an integrated study. In *Ambio* (pp. 91–95).

[90]. Vishwakarma, C. A., Thakur, S., Rai, P. K., Kamal, M. S., & Mukherjee, S. (2016). Changing land trajectories: a case study from India using a remote sensing-based approach. *Eur J Geogr*, *7*(2), 61–71.

[91]. Vivekananda, G. N., Swathi, R., & Sujith, A. (2021). Multi-temporal image analysis for LULC classification and change detection. *European Journal of Remote Sensing*, *54*(sup2), 189–199.

[92]. Vuolo, F., Neuwirth, M., Immitzer, M., Atzberger, C., & Ng, W.-T. (2018). How much does multi-temporal Sentinel-2 data improve crop type classification? *International Journal of Applied Earth Observation and Geoinformation*, *72*, 122–130.

[93]. Waldner, F., &Defourny, P. (2017). Where can pixel counting area estimates meet user-defined accuracy requirements? *International Journal of Applied Earth Observation and Geoinformation*, *60*, 1–10.

[94]. Wulder, M. A., Loveland, T. R., Roy, D. P., Crawford, C. J., Masek, J. G., Woodcock, C. E., Allen, R. G., Anderson, M. C., Belward, A. S., & Cohen, W. B. (2019). Current status of Landsat program, science, and applications. *Remote Sensing of Environment*, *225*, 127–147.

[95]. Xu, W. (2019). A LM-2D Launches GF-6 Satellite. 中国航天 (英文版) *19*(2), 60.

[96]. Yang, A., Zhong, B., Hu, L., Wu, S., Xu, Z., Wu, H., Wu, J., Gong, X., Wang, H., & Liu, Q. (2020). Radiometric cross-calibration of the wide field view camera onboard gaofen-6 in multispectral bands. *Remote Sensing*, *12*(6), 1037.

[97]. Zeb, A., Hamann, A., Armstrong, G. W., & Acuna-Castellanos, D. (2019). Identifying local actors of deforestation and forest degradation in the Kalasha valleys of Pakistan. *Forest Policy and Economics*, *104*, 56–64.

[98]. Zhang, C., Chen, Y., Yang, X., Gao, S., Li, F., Kong, A., Zu, D., & Sun, L. (2020). Improved remote sensing image classification based on multi-scale feature fusion. *Remote Sensing*, *12*(2), 213.